Heliyon 6 (2020) e04457

Contents lists available at ScienceDirect

Heliyon

journal homepage: www.cell.com/heliyon

Research article

Photolysis, tautomerism and conformational analysis of dehydroacetic acid and a comparison with 2-hydroxyacetophenone and 2-acetyl-1,3-cyclohexanodione

María Victoria Cooke [a], Guillermo M. Chans [b], Gustavo A. Argüello [a], Walter José Peláez [a,*]

[a] INFIQC-CONICET-Dpto. de Fisicoquímica, Facultad de Ciencias Químicas, Universidad Nacional de Córdoba, Ciudad Universitaria, Córdoba, X5000HUA, Argentina
[b] Tecnologico de Monterrey, Escuela de Ingeniería y Ciencias, Av. Carlos Lazo 100, Mexico City, 01389, México

ARTICLE INFO

Keywords:
Physical chemistry
Dehydroacetic acid
Photodegradation
Tautomerism

ABSTRACT

The purpose of this work was to determine the tautomerism, the conformational analysis and photoreactivity of dehydroacetic acid (DHAA, **1**). For that reason, the photolysis of DHAA (**1**) was performed at 254 nm and compared with two structurally similar compounds: 2-hydroxyacetophenone (HAP, **2**) and 2-acetyl-1,3-cyclohexanodione (ACH, **3**). We confirmed the degradation of **1** to acetic acid and we propose a mechanism on the assumption that a [2+2] cyclodimerization occurs (after UV light absorption) followed by some consecutive Norrish Type I cleavages, affording ketenes that end-up in acetic acid. The UV absorption study was conducted for all three compounds to gain insight about their electronic transitions, both experimentally and with computational simulations using TDDFT (B3LYP/6-31+G(d,p)) methods. A detailed analysis of the different tautomers and isomers that can be present in solution and the MOs involved in the electronic transitions was also achieved. The HOMO→LUMO transition was the least energetic optically active transition for **1** and **2**, whereas **3** was recognized to have a HOMO-1→LUMO transition. These transitions were all of n→π* character.

1. Introduction

Dehydroacetic acid (DHAA, **1**, Figure 1, left) is an organic compound derived from the condensation of ethyl acetoacetate [1], which is widely used as fungicide, herbicide and preservative. This is due to some interesting properties such as good stability, low volatility [2], and powerful antimicrobial effect against yeasts, molds and bacteria. Among other properties, it is a Vitamin C stabilizer, particularly useful in the food industry [3] and as anti-enzyme agent that found application in toothpastes to reduce pickle bloating [4]. In addition, it is commonly used in the syntheses of metal complexes [5] and derivatives such as piranopirazoles [6, 7]. Another important application is its widespread use in the cosmetics industry that exposes **1** to direct sunlight when used for skin face powders and creams. Izawa *et al.* [8] was the first group to report on the effect of light upon **1** and found that it acts as photosensitizer, promoting photoisomerization of aldrin and dieldrin after irradiation with a Xe lamp and a cutoff filter below 290 nm. In this study, we explore a comprehensive research about the photochemical degradation/reaction of **1** at 254 nm due to the versatility of its usage and the lack of related works. To better comprehend its photochemical behavior, two similarly structured compounds were also studied; HAP **2** (Figure 1, center) and ACH **3** (Figure 1, right). Compound **2** is generally used in the synthesis of Schiff bases to later use these bases as ligands in metal complexes [9] which may present antifungal and antibacterial activities [10], and ACH has been used as a precursor in heterocyclic compounds synthesis [11] and as ligand in iridium [12] and iron(III) [13] complexes. The structural similarity sought in this work has to do with the presence of the same chromophores (β-carbonyl groups) as well as the possibility of rapid interchange between keto and enol tautomers. Precisely, a recent study by Sarkar *et al.* [14] reported that HAP undergoes excited state intramolecular proton transfer (ESIPT) on their singlet excited state to form the corresponding keto tautomer, which is not stable and reverts to its enol tautomer, either via ground-state intramolecular proton transfer (GSIPT) or by interacting with the solvent. Finally, this report also presents a UV absorption study (both experimental and computational) to understand the nature of the electronic transition involved at that wavelength of irradiation.

* Corresponding author.
E-mail address: walter.pelaez@unc.edu.ar (W.J. Peláez).

https://doi.org/10.1016/j.heliyon.2020.e04457
Received 6 May 2020; Received in revised form 16 June 2020; Accepted 10 July 2020

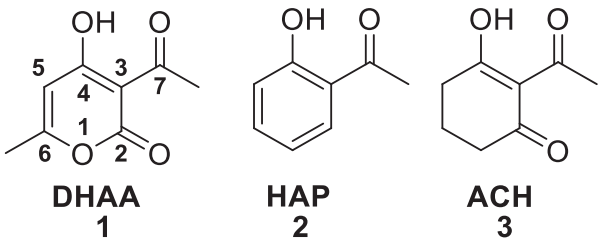

Figure 1. Compounds studied in this work.

2. Materials and methods

2.1. Materials

Compound **1** (98%) was supplied by Aldrich Chemical Company whereas **2** (99%) and **3** (99%) by Sigma-Aldrich. Acetonitrile (ACN, HPLC 99.5%) and ethanol (99.8%) were provided by Sintorgan and Merck, respectively. Water was purified using a reverse osmosis RIOS 5 and Synergy (Millipore) (resistivity 18.2 MΩcm, DOC <0.1 mg L^{-1}). Acetone-d_6 and acetonitrile-d_3 were used to obtain the NMR spectra, both provided by Sigma-Aldrich. All solvents and chemicals were used as received without further purification.

2.2. Irradiation and thermal studies methods

Irradiation was conducted using four low pressure mercury lamps emitting at 254 nm. The reaction was conducted in a quartz cell with an optical path of 1 cm open to the atmosphere.

The solutions were prepared in ACN and the reaction cell was thermostatted at 25 °C. UV-visible spectra were recorded on an Agilent 8354 spectrophotometer. Thermal stability studies were conducted at 50 °C and were followed by UV-Vis spectroscopy for 1 h taking measurements every 5 min.

FT-IR spectra were recorded with a FTIR Bruker IFS28 spectrometer (2 cm^{-1} resolution and 4000-400 cm^{-1} interval) using KBr disks painted either with the photolysis crude before or after irradiation. NMR spectra were obtained with a 400 MHz Bruker Advance II spectrometer.

3. Theoretical calculations

The ground state geometry of all possible tautomers and conformers for **1**, **2** and **3** were fully optimized employing the Gaussian09 program suite [15], in a similar way to our previous works [16]. The hybrid B3LYP functional method [17, 18] was used in combination with the 6-31+G(d,p) basis set for the expansion of the Kohn-Sham orbitals for all the atoms. The polarizable conductor calculation model of solvation (CPCM) was used [19, 20]. The gradient threshold for geometry optimization was 4.5×10^{-4} Hartree/Bohr. A frequency analysis at the same level of theory was used to verify that they correspond to a minimum in the potential energy surface. Electronic, translational, vibrational and rotational contributions to the partition function were determined and a population distribution was calculated for every compound according to Boltzmann distribution equation [21]. MOs were also obtained, and their composition was calculated with the GaussSum software [22].

The excited state properties were calculated with the time-dependent density functional (TDDFT) formalism. Whereas semi-empirical approaches have been used to study other systems [23], TDDFT [24, 25, 26] is based on first principles, which enables the analysis of excitation energies, oscillator strengths and polarizabilities of larger systems. TDDFT in combination with the B3LYP hybrid functional and the 6-31+G(d,p) basis set has previously been shown to provide accurate energies for excited states within 0.2 eV (5 kcal mol^{-1}) [27]. Theoretical coefficients (ε_{calc}) have been calculated as [28]:

$$\varepsilon_{calc} = f \times 2.699 \times \frac{10^4}{b} \quad (1)$$

where b is the band width and f the oscillator strength.

4. Results and discussion

4.1. Tautomerism and conformational analysis

A thorough conformational analysis of all the possible isomers and conformers for **1**, **2** and **3** was performed using the Gaussian09 Program [15]. This was implemented both in vacuum and in ACN employing an implicit solvent. Computational conformational studies as well as energetic and population characteristics of the different isomers of **1**, **2** and **3** are presented in Supplementary data in pages S4–S54 and Tables S2–S4. The most stable structures are the enolic form in all cases. The contribution of diketo or triketo tautomeric forms are negligible. We believe that the low stability of these forms is because the ring aromaticity is lost in **2**, whereas an absence of conjugated bonds is involved in **1** and **3**.

For the most stable forms there are two possible structures, the *endo*-cyclic (enol **a**) and the *exo*-cyclic (enol **b**), which are presented in Figure 2a. The *endo* form is always more stable than the *exo*. Nevertheless, the proportion of both enol tautomers for each compound differs. Regarding compound **1**, the *endo*-**a** structure has a higher conjugation, giving an *endo*:*exo* proportion of 91:9. In **2**, *endo*-**a** form is present exclusively, in view of the fact that the *exo* compound has lost its aromaticity. Finally, for **3**, both *endo* and *exo* structures are equally conjugated (*endo*:*exo* 55:45, respectively).

4.2. Analysis of MO formation

As seen in Figure 2b, morphologies, types and energies of the MOs for the *endo*-enols-**a** conformations are presented. The MOs compositions were obtained using the GaussSum software [22].

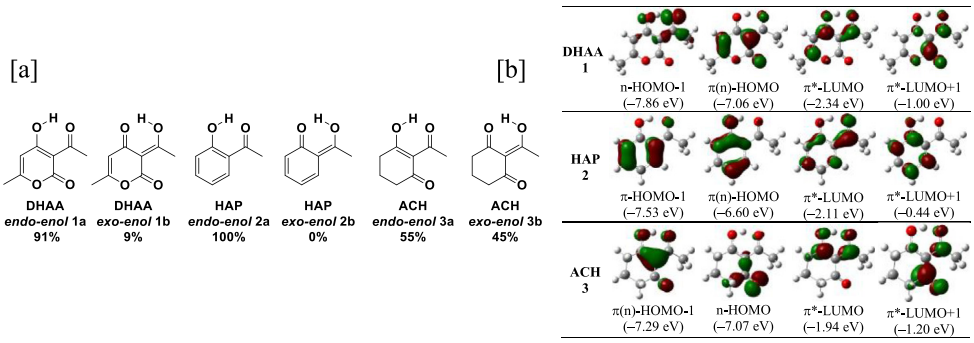

Figure 2. [a] *Endo*- and *exo*-enol structures and population percentages; [b] shapes, types and energies (in parenthesis) of the *endo*-enols-**a**'s MOs as calculated by DFT (B3LYP/6-31+G(d,p)) method in ACN (isovalue = 0.06).

[a]

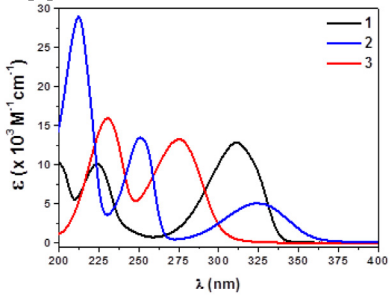

[b]

Compound	ACN		EtOH		H_2O	
	λ (nm)	ε ($M^{-1}cm^{-1}$)	λ (nm)	ε ($M^{-1}cm^{-1}$)	λ (nm)	ε ($M^{-1}cm^{-1}$)
DHAA 1	224	10300	224	10180	226	11550
	312	12900	310	12020	305	10470
HAP 2	212	28500	213	41900	210	17900
	251	12750	251	19900	253	9650
	324	4760	325	7660	323	3060
ACH 3	230	15800	232	7760	236	9630
	275	13400	274	6520	272	12180

Figure 3. [a] UV spectra in ACN; [b] λ_{max} (nm) and ε ($M^{-1}cm^{-1}$) in different solvents.

The occupied MOs HOMO-1 of **1** and HOMO of **3** present a nodal plane perpendicular to the ring moiety and are attributed to non-bonding MOs (97 and 99%, respectively). On the other hand, in the HOMO of **1** and the HOMO-1 of **3**, there is an electronic contribution to the MO from both the π electrons of the double bonds and the lone-pair electrons of the oxygens (29 and 40%, respectively). In regard to **2**, both HOMO-1 and HOMO orbitals present a nodal plane parallel to the plane of the ring. The former presents a contribution of 91% of the MOs from the ring double bonds whereas for the latter is only 78% plus a lone-pair contribution (21%) from the oxygen. This contribution to the MO increases as the conjugated π system decreases, with **2** having the lowest and **3** having the highest contribution to an n type MO.

For all compounds, both the LUMO and LUMO+1 orbitals present a π* symmetry, in which the main contribution comes from the carboxylic and carbon-carbon double bonds.

4.3. UV absorption measurements

UV spectra of **1**, **2** and **3** were recorded in ACN (Figure 3a), EtOH and H_2O in order to obtain information about the nature of the transitions involving the main bands (Experimental UV spectra of **1**, **2** and **3** in different solvents are given in Figures S1–S3 in Supplementary data). The spectra band maxima were determined for each of them and corroborated with second derivative spectra. Their molar absorption coefficients were also calculated and presented in Figure 3b.

Three distinct absorption bands, which decrease in intensity as wavelength increases can be seen for **2**, whereas only two absorption bands are observed for **1** and **3**. When changing polarity of the solvent, no apparent shift was discerned for the three maxima of **2**. Therefore, the nature of the electronic transitions could not be straightforwardly resolved. Nonetheless, a hyperchromic effect was noted in ethanol. In contrast, a bathochromic shift of the most energetic band maxima was identified in **1** and **3** when the polarity of the solvent increased, which is typical for π→π* electronic transitions. Similarly, a hypsochromic shift for the lowest energy band was also detected, denoting an n→π* electronic transition. It is widely known that the behavior in π→π* electronic transitions can be attributed to an increase in the polarity of the molecule in the excited state which is stabilized through dipole-dipole interactions. On the other hand, the polarity's increase of the solvent in n→π* electronic transitions stabilizes the fundamental state via solvation of the non-bonding electron pair [29].

4.4. UV absorption calculations

Given that the nature of the electronic transitions was not discernible in all cases, TDDFT calculations were used to simulate the UV spectra and to ascertain which MOs are involved in each transition. The B3LYP functional method was used to carry out these calculations with 6-31+G(d,p) as a basis set. These calculations were only performed in ACN because there is no noticeable trend of the shifts using different solvents as it was previously seen and reported [30] (UV Spectra of **1**, **2** and **3** and transitions of the monoenols obtained by calculations are presented in Figure S10a-c in Supplementary data). Table 1 lists for the *endo/exo*-enols their oscillator strengths and compares the calculated absorption coefficients and wavelengths with the experimental ones. It can be observed a remarkable accordance between them. The orbitals involved and the type of transition are also listed.

All four electronic transitions, involving the four MOs previously discussed, are permitted in **2**, considering that they do not present any restrictions in their symmetry. On the other hand, the HOMO-1 of **1** and HOMO of **3** are constricted by symmetry and their possible electronic transitions are therefore optically inactive. Additionally, in all compounds, the electronic transitions are π→π*, except for the least energetic ones. In the latter case, the assignment could be n→π* (in accordance

Table 1. Experimental (solvent: ACN) and theoretical (TDDFT) characteristics of **1**, **2** and **3**.

Entry	Compound (% *endo/exo*-enol)	Experimental[a]		Calculated (TDDFT)[b]						Transition (% *endo/exo*-enol)[c]	Assignment
		λ_{max}^{exp}	ε_{exp}	*Endo*-enol			*Exo*-enol				
				λ_{max}^{calc}	*f*	ε_{calc}	λ_{max}^{calc}	*f*	ε_{calc}		
1	**1** (91/9)	224	10300	224	0.17	11300	225	0.04	2600	H→L+1 (82/96)	π→ π*
2		312	12900	298	0.31	20800	292	0.26	17900	H→L (98/96)	n→ π*
3	**2** (100/0)	212	28500	202	0.21	14100	–	–	–	H-1→L+1 (40); H→L+3 (40)	π→ π*
4				214	0.24	16300	–	–	–	H→L+1 (75)	π→ π*
5		251	12750	250	0.26	17400	–	–	–	H-1→L (90)	π→ π*
6		324	4760	318	0.11	7200	–	–	–	H→L (96)	n→ π*
7	**3** (55/45)	230	15800	225	0.30	20000	224	0.29	19500	H-1→L+1 (92/86)	π→ π*
8		275	13400	253	0.27	18200	258	0.26	17500	H-1→L (96/97)	n→ π*

[a] Peak maxima were determined using a second derivative-based method.
[b] TD-B3LYP 6-31+G(d,p).
[c] H-highest occupied MO (HOMO), L-lowest unoccupied MO (LUMO).

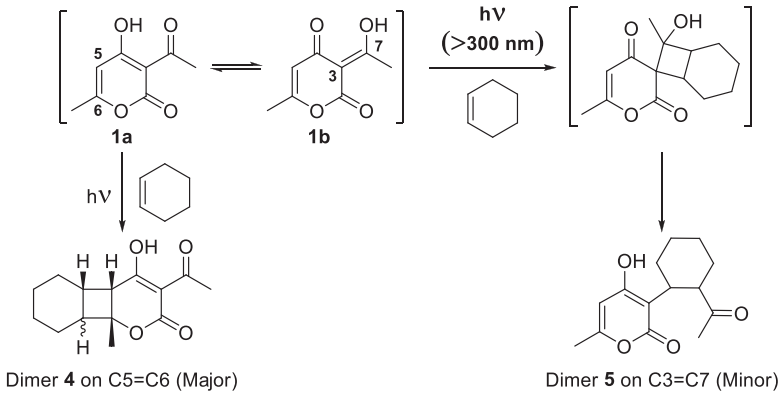

Scheme 1. [2+2]-cycloaddition of **1** with cyclohexene from tautomers **1a** and **1b**.

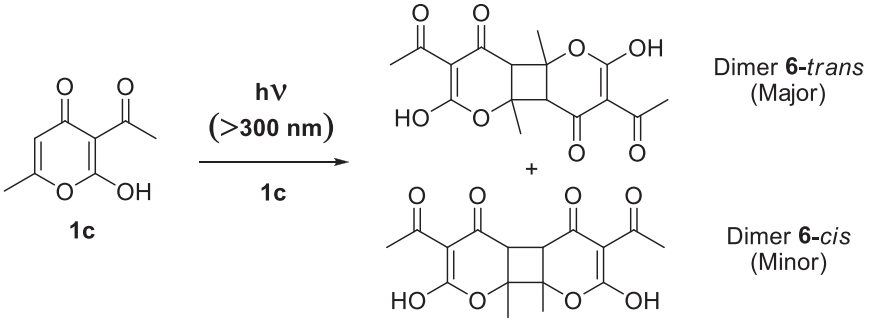

Scheme 2. [2+2]-cyclodimerization of **1c** tautomer previously reported.

with the experimental evidence) because a lone pair electron from the oxygens is the most likely to transfer to the LUMO for the least energetic electronic transition.

4.5. Photolysis of DHAA

Photochemical reactions of **1** at wavelengths over 300 nm have been described in the review published by Jilalat *et al.* [31] They reported that if the photoreaction (visible light) is carried out with an excess of cyclohexene, a mixture of cycloadducts is obtained, Scheme 1. The products were identified via ^{1}H-NMR and they proposed these compounds came from two different [2+2]-cycloadditions; one on the C5=C6 (*endo*-double bond) and the second on the C3=C7 (*exo*-double bond) which correspond to our enols **1a** and **1b**, respectively.

On the other hand, De Vaugelade *et al*, [32] performed the photochemical degradation of **1** with a Xenon arc lamp using a natural light filter (for a realistic reproduction of the solar spectrum). They detected four photoproducts in the ACN solution after irradiation, two of them identified as dimers coming from its own [2+2]-cycloaddition (Scheme 2), and relative amounts estimated by integrating the chromatographic peaks on the GC/MS.

The authors, though, proposed that all products come from tautomer **1c**, which is practically absent in ACN solution, as it was discussed. This contradiction could probably be understood on account of the experimental technique used, since the identification was done only through MS. It is noteworthy to mention that our work is the first report about the population analyses and UV degradation of **1** at wavelengths <300 nm. In our case, the photolysis was accomplished at 254 nm and it was followed using UV spectroscopy. As it is possible to see in Figure 4, the intensity of both absorption bands diminishes as time goes by during the photolysis; nevertheless, no new absorption bands were found. On account of these results, we could prematurely conclude that the photodecomposition products do not possess a chromophore moiety that

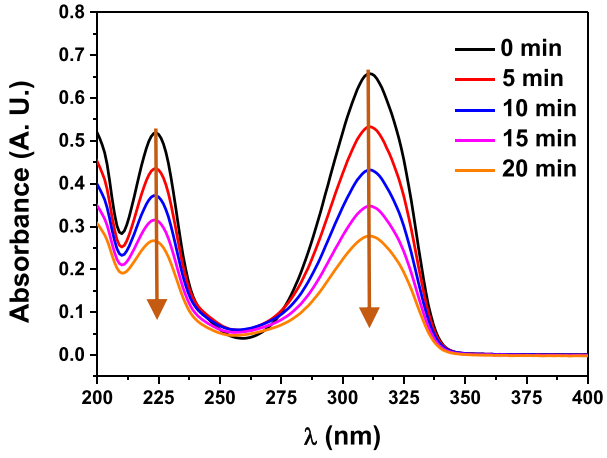

Figure 4. Photolysis of **1** in ACN (303 K) and air atmosphere at 254 nm followed via UV spectroscopy.

absorbs in the UV-Vis region of the electromagnetic spectrum. In addition, photolysis at different temperatures showed that the thermal contribution to decomposition is negligible in the temperature interval tested (293–313 K). FTIR spectra of **1** before and after the photolysis revealed the appearance of a vibrational band corresponding to O–H stretching (FTIR (KBr) spectrum of DHAA **1** is given in Figure S6 in Supplementary data).

Insight into the mechanistic aspects of the photodegradation of **1** is gained by comparing the evolution of spectral features in the photolysis of two similar structures (**2** and **3**) in the same experimental conditions. No significant decay of their absorption bands was detected during the

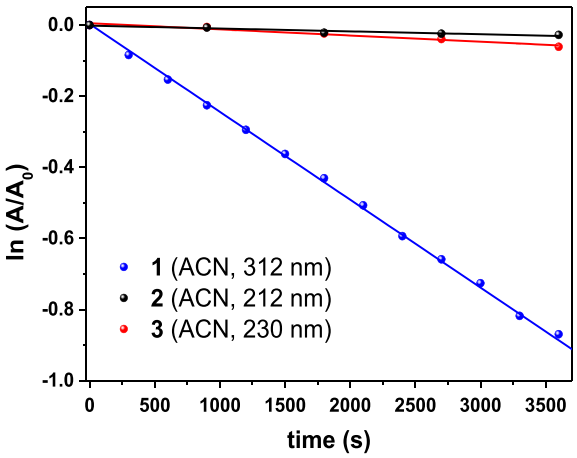

Figure 5. Ln(A/A$_0$) vs time of **1**, **2** and **3** in ACN.

irradiation period for any compound. In fact, the decay rate shows significant differences (Figure 5). Particularly, compound **1** degraded rapidly whereas **2** and **3** did not (decay rates of the photolysis of **1**, **2** and **3** and their ratio are given in Table S1 in Supplementary data).

A comparison of the decay rates showed that the degradation of **2** and **3** are 30 and 15 times slower than for **1**, respectively. Compound **2** has been reported to undergo ESIPT [14] on its singlet excited state to form the corresponding *exo*-enol tautomers. In spite of being unstable, they are able to regenerate their enol tautomers via GSIPT or by interacting with the solvent. In our experiments performed at 254 nm (irradiation in nitrogen- and oxygen-saturated ACN solutions), **2** and **3** resulted to be photostable leading us to think that the same photochemical channels (ESIPT followed by GSIPT) will be involved, Scheme 3.

As denoted previously, the only compound that suffers decomposition at 254 nm is **1**. Bearing in mind that the main difference between the three structures is the heterocyclic moiety, we postulate that the C–O bond of the lactone plays an important role in its photodegradation. All photolysis reactions were followed by ^{1}H-NMR in deuterated acetonitrile and all of them unveiled the formation of acetic acid as the unique decomposition product (^{1}H-NMR and photolysis ^{1}H-NMR study of DHAA

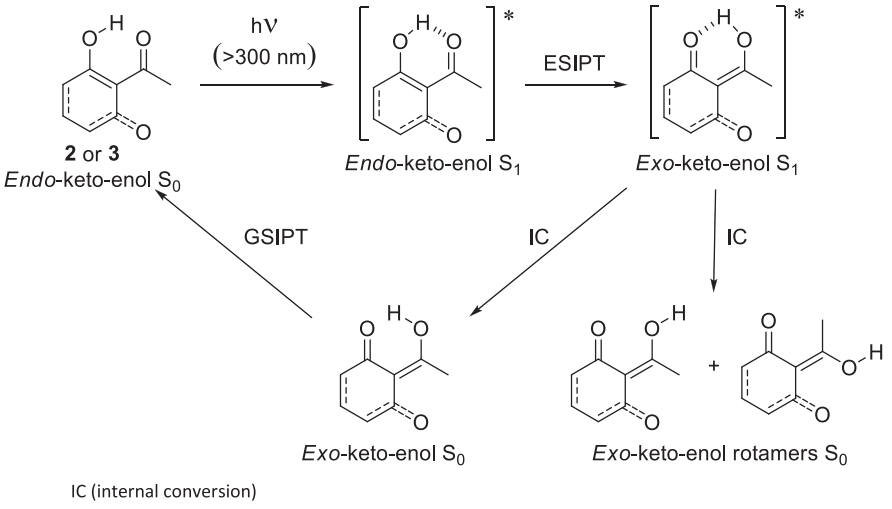

Scheme 3. Photo-tautomerization mechanism proposed for **2** and **3**.

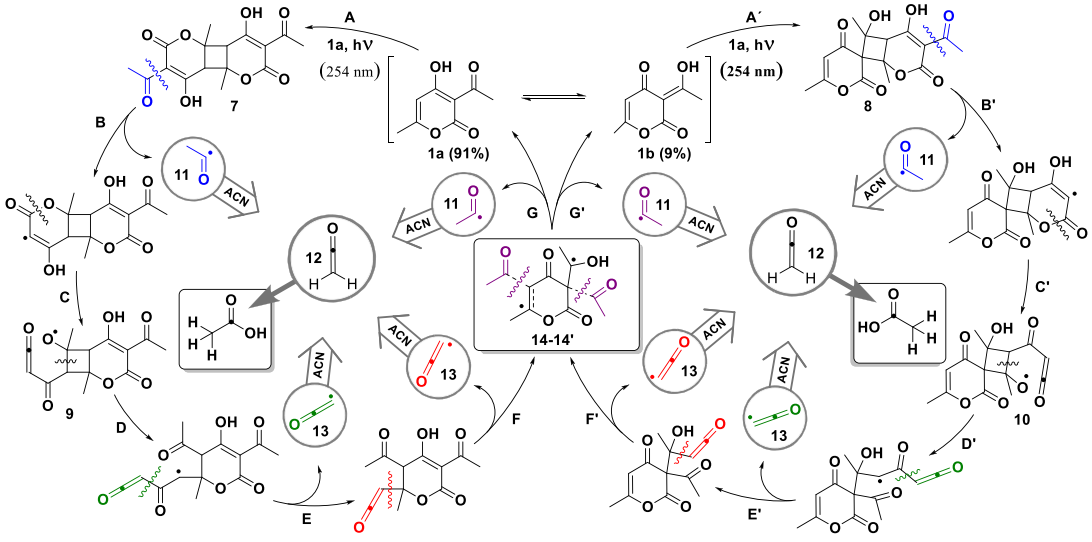

Scheme 4. Proposed photodecomposition mechanism for **1** in ACN at 254 nm.

1 spectra are given in Figures S4–S5 in Supplementary data). Additionally, the possible interaction of oxygen in the mechanism of photodegradation was analyzed via an indirect singlet oxygen measurement method with cysteine [33]. This essay confirmed that there was no energy transfer involved in the process and that neither the presence nor the absence of oxygen present a remarkable difference in the resulting product. Moreover, the photodecomposition of **1** takes place from the singlet-excited state and the intersystem crossing to the triplet excited state is insignificant with respect to the final outcome.

As denoted previously by Jilalat *et al.* [30] and De Vaugelade *et al.* [32], a [2+2]-cyclodimerization of **1** is a probable light promoted first step at wavelengths lower than 300 nm. With the exception of these recent works, there are, to the best of our knowledge, no previous mechanistic studies on the photoreaction of **1** under UV-light (254 nm). In this work, we propose to gather all the information available (ours and previous works), to design a mechanism of the photodegradation of **1** at 254 nm to yield acetic acid as unique photostable product, just as the one presented in Scheme 4. Here we suggest that, after the photoabsorption, the [2+2]-cyclodimerization reaction occurs from both major tautomers, **1a** and **1b**, yielding two isomeric cyclobutanes fused differently, structures 7-*trans* (*endo*) and 8-*trans* (*exo*), respectively (paths A and A′, Scheme 4). These unstable dimers undergo a Norrish Type I cleavage (NTIC), followed by a lactone ring opening, where bicyclic radical compounds bearing a ketene group as substituent are formed (compounds **9** and **10**, paths B–C and B′-C′, respectively). It is important to note that, similarly, through the resulting acyl radicals (**11**), other ketene is also formed (ethenone **12**, CH_2=C=O), which in turn hydrolyzes to acetic acid. Unstable radicals **9** and **10** have a cyclobutane ring opening reaction, which affords, by two consecutive fragmentations, ketene radicals **13** (paths D-F and D′-F′). After hydrogen abstraction from the solvent, they hydrolyze to acetic acid. In the same way, acetylated DHAA radicals are formed (ADHAAs$^{\bullet}$, **14** and **14′**), that in a subsequent fragmentation re-start the cyclic photoinduced degradation (paths G and G′ respectively).

Acetic acid is an ubiquitous organic acid and is present in the atmosphere at concentrations of few parts per billion by volume [34]. Previous studies have shown that the pyrolysis of biomass, produces various organic compounds and generate ketene (ethenone **12**) as a major byproduct [35]. It is well known that the hydrolysis of **12** generates acetic acid, therefore the photodegradation of **1** could potentially lead to an additional source of tropospheric acetic acid [36].

5. Conclusions

During the photochemical study at 254 nm of the three carbonyl compounds, only **1** is degraded whereas **2** and **3** are photostable. The decomposition is likely to occur through a [2+2]-cyclodimerization after UV light absorption (254 nm) from both major tautomers, wherein the *endo*-enol (90%) is more stable than the *exo*-enols due to hydrogen bond stabilization, as shown by the population distribution analysis. In addition, the size of the π-system plays a crucial role in the proportion of *endo*- and *exo*-cyclic enols, in which the *exo*-cyclic rises as the π-system size diminishes. As a very first-time characterization, the absorption and the electronic transitions for every tautomer were calculated and it was determined that the nature of the lowest energy transition type is n→π* for all compounds. Furthermore, photolysis of the dehydroacetic acid **1** at 254 nm generates ethenone **12**, which potentially could be other source of tropospheric acetic acid.

Declarations

Author contribution statement

Maria V. Cooke: Performed the experiments; Analyzed and interpreted the data.

Guillermo M. Chans: Analyzed and interpreted the data; Contributed reagents, materials, analysis tools or data.

Gustavo A. Argüello: Conceived and designed the experiments.

Walter J. Peláez: Conceived and designed the experiments; Analyzed and interpreted the data; Contributed reagents, materials, analysis tools or data; Wrote the paper.

Funding statement

Walter José Peláez was supported by Consejo Nacional de Investigaciones Científicas y Técnicas - CONICET, Argentina (PIP: 11220170100423CO), Fondo para la Investigación Cientìfica y Tecnológica - FonCyT (PICT-2017-1555) and Secretaría de Ciencia y Tecnología - Universidad Nacional de Córdoba (SeCyT: Nº411/18).

Competing interest statement

The authors declare no conflict of interest.

Additional information

Supplementary content related to this article has been published online at https://doi.org/10.1016/j.heliyon.2020.e04457.

References

[1] M. Zucolotto Chalaça, J.D. Figueroa-Villar, J.A. Ellena, E.E. Castellano, Synthesis and structure of cadmium and zinc complexes of dehydroacetic acid, Inorg. Chim. Acta. 328 (1) (2002) 45–52.

[2] E. Mikami, T. Goto, H. Matsumoto, M. Nishida, Simultaneous analysis of dehydroacetic acid, benzoic acid, sorbic acid and salicylic acid in cosmetic products by solid-phase extraction and high-performance liquid chromatography, J. Pharmaceut. Biomed. Anal. 28 (2) (2002) 261–267.

[3] Y.-G. Zhao, M.-Q. Cai, X.-H. Chen, S.-D. Pan, S.-S. Yao, M.-C. Jin, Analysis of nine food additives in wine by dispersive solid-phase extraction and reversed-phase high performance liquid chromatography, Food Res. Int. 52 (1) (2013) 350–358.

[4] A.S. Al-Aousi, M.R. Shehata, M.M. Shoukry, S.A. Hassan, N. Mahmoud, Coordination properties of dehydroacetic acid – binary and ternary complexes, J. Coord. Chem. 61 (12) (2008) 1906–1916.

[5] D.M. Fouad, A. Bayoumi, M.A. El-Gahami, S.A. Ibrahim, A.M. Hammam, Synthesis and thermal studies of mixed ligand complexes of Cu(II), Co(II), Ni(II) and Cd(II) with mercaptotriazoles and dehydroacetic acid, Nat. Sci. 2 (8) (2010) 817–827.

[6] V.Y. Sosnovskikh, B.I. Usachev, A.G. Blinov, M.I. Kodess, New derivatives of dehydroacetic acid: synthesis of 2-polyfluoroalkyl-7-methylpyrano[4,3-b]pyran-4,5-diones, Mendeleev Commun. 11 (1) (2001) 36–38.

[7] R. Prakash, A. Kumar, S.P. Singh, R. Aggarwal, O. Prakash, Dehydroacetic acid and its derivatives in organic synthesis: Synthesis of some new 2-substituted-4- (5-bromo-4-hydroxy-6-methyl- 2H-pyran-2-one-3-yl)thiazoles, Indian J. Chem. 46B (10) (2007) 1713–1715. http://nopr.niscair.res.in/handle/123456789/752.

[8] T. Izawa, K. Nakayama, N. Uchida, K. Nojima, Photoreactivities of the Antiseptics Dehydroacetic Acid and Sodium Dehydroacetate Used in Cosmetics, Chem. Pharm. Bull. 66 (5) (2018) 581–584.

[9] M.M. Conejo, P. Ávila, E. Álvarez, A. Galindo, Synthesis and structure of nickel and copper complexes containing the N-allyl-o-hydroxyacetophenoniminato ligand and the application of copper complex as catalyst for aerobic alcohol oxidations, Inorg. Chim. Acta. 455 (2017) 638–644.

[10] S.S. Swathy, R.S. Joseyphus, V.P. Nisha, N. Subhadrambika, K. Mohanan, Synthesis, spectroscopic investigation and antimicrobial activities of some transition metal complexes of a [(2-hydroxyacetophenone)-3-isatin]-bishydrazone, Arabian J. Chem. 9 (2) (2016) S1847–S1857.

[11] I. Strakova, A. Strakovs, M. Petrova, 1-(2-Quinoxalyl)-, 1-[3,5-Di(trifluoromethyl) phenyl]-, 1-(2-Carboxyphenyl)-, and 1-Ethoxycarbonyl-4-oxo-4,5,6,7-tetrahydroindazoles, Chem. Heterocycl. Compd. 38 (4) (2002) 429–433.

[12] D.-U. Kim, S.-H. Paik, S.-H. Kim, Y.-H. Tak, S.-D. Kim, K.-D. Kim, K.-H. Kim, T.-H. Ko, U.-C. Yoon, Y.-S. Han, Y.C. Jeong, L.S. Park, Development of novel red phosphorescent iridium complex with phenyl-isoquinoline ligand for organic electroluminescent device, Curr. Appl. Phys. 6 (4) (2006) 805–807.

[13] C.A. Blanco, I. Caballero, A. Rojas, M. Gomez, J. Alvarez, Chelation of aqueous iron(III) by 2-acetyl-1,3-cyclohexanedione and beer ageing, Food Chem. 81 (4) (2003) 561–568.

[14] S.K. Sarkar, G.K. Weragoda, R.A.A.U. Ranaweera, A.D. Gudmundsdottir, Phototautomerization on the singlet and triplet surface in *o*-hydroxyacetophenone derivatives in polar solvents, J. Phys. Chem. B 119 (6) (2015) 2668–2676.

[15] M.J. Frisch, G.W. Trucks, H.B. Schlegel, G.E. Scuseria, M.A. Robb, J.R. Cheeseman, G. Scalmani, V. Barone, B. Mennucci, G.A. Petersson, H. Nakatsuji, M. Caricato, X. Li, H.P. Hratchian, A.F. Izmaylov, J. Bloino, G. Zheng, J.L. Sonnenberg, M. Hada, M. Ehara, K. Toyota, R. Fukuda, J. Hasegawa, M. Ishida, T. Nakajima, Y. Honda,

O. Kitao, H. Nakai, T. Vreven, J.A. Montgomery Jr., J.E. Peralta, F. Ogliaro, M. Bearpark, J.J. Heyd, E. Brothers, K.N. Kudin, V.N. Staroverov, T. Keith, R. Kobayashi, J. Normand, K. Raghavachari, A. Rendell, J.C. Burant, S.S. Iyengar, J. Tomasi, M. Cossi, N. Rega, J.M. Millam, M. Klene, J.E. Knox, J.B. Cross, V. Bakken, C. Adamo, J. Jaramillo, R. Gomperts, R.E. Stratmann, O. Yazyev, A.J. Austin, R. Cammi, C. Pomelli, J.W. Ochterski, R.L. Martin, K. Morokuma, V.G. Zakrzewski, G.A. Voth, P. Salvador, J.J. Dannenberg, S. Dapprich, A.D. Daniels, O. Farkas, J.B. Foresman, J.V. Ortiz, J. Ioslowski, D.J. Fox, Gaussian 09, Revision B.01, Gaussian, Inc., Wallingford CT, 2010.

[16] G.M. Chans, E.L. Moyano, M.T. Baumgartner, NMR and computational studies on tautomerism of 3-hydroxy-2-(2-thienylcarbonyl)cyclohex-2-en-1-one, J. Mol. Struct. 1059 (2014) 176–184.

[17] A.D. Becke, Density-functional thermochemistry. III. The role of exact exchange, J. Chem. Phys. 98 (7) (1993) 5648–5652.

[18] C. Lee, W. Yang, R.G. Parr, Development of the Colle-Salvetti correlation-energy formula into a functional of the electron density, Phys. Rev. B 37 (2) (1988) 785–789.

[19] V. Barone, M. Cossi, Quantum calculation of molecular energies and energy gradients in solution by a conductor solvent model, J. Phys. Chem. A 102 (11) (1998) 1995–2001.

[20] M. Cossi, N. Rega, G. Scalmani, V. Barone, Energies, structures, and electronic properties of molecules in solution with the C-PCM solvation model, J. Comput. Chem. 24 (6) (2003) 669–681.

[21] P. Atkins, J. de Paula, Atkins' Physical Chemistry, seventh ed., Oxford University Press, 2002.

[22] N.M. O' Boyle, A.L. Tenderholt, K.M. Langner, cclib: A library for package-independent computational chemistry algorithms, J. Comput. Chem. 29 (5) (2008) 839–845.

[23] A.R. Tameev, Z. He, G.H.W. Milburn, A.A. Kozlov, V. Vannikov, A. Puchala, D. Rasala, Electron drift mobility in polystyrene doped with bispyrazolopyridine derivatives, Appl. Phys. Lett. 81 (6) (2002) 969–971.

[24] G. Ricciardi, A. Rosa, S.J.A. van Gisbergen, E.J. Baerends, A Density Functional Study of the Optical Spectra and Nonlinear optical properties of heteroleptic tetrapyrrole sandwich complexes: the porphyrinato−porphyrazinato−zirconium(IV) complex as a case study, J. Phys. Chem. A 104 (3) (2000) 635–643.

[25] S.J.A. van Gisbergen, J.A. Groeneveld, A. Rosa, J.G. Snijders, E.J. Baerends, Excitation energies for transition metal compounds from time-dependent density functional theory. applications to MnO_4^-, $Ni(CO)_4$, and $Mn_2(CO)_{10}$, J. Phys. Chem. 103 (34) (1999) 6835–6844.

[26] A. Rosa, E.J. Baerends, S.J.A. van Gisbergen, E. van Lenthe, J.A. Groeneveld, J.G. Snijders, Electronic spectra of $M(CO)_6$ (M = Cr, Mo, W) revisited by a relativistic TDDFT approach, J. Am. Chem. Soc. 121 (44) (1999) 10356–10365.

[27] J. Llano, L.A. Eriksson, Oxidation pathways of adenine and guanine in aqueous solution from first principles electrochemistry, Phys. Chem. Chem. Phys. 6 (19) (2004) 4707–4713.

[28] H. Baumann, R.E. Martin, F. Diederich, PM3 geometry optimization and CNDO/S-CI computation of UV/Vis spectra of large organic structures: Program description and application to poly(triacetylene) hexamer and taxotere, J. Comput. Chem. 20 (4) (1999) 396–411.

[29] C. Reichardt, Solvent effects on the absorption spectra of organic compounds. Solvents and Solvent Effects in Organic Chemistry, third ed., Wiley-VCH, 2004. Chapter 6.

[30] M.V. Cooke, I. Malvacio, W.J. Peláez, A.J. Pepino, M.R. Mazzieri, G.A. Argüello, TD-DFT calculations of UV absorption bands and their intensities in the spectra of some tetrahydroquinolines, RSC Adv. 5 (5) (2015) 26255–26262.

[31] A.E. Jilalat, W.H.A.H. Al-Garadi, K. Karrouchi, E.M. Essassi, Dehydroacetic acid (part 1): chemical and pharmacological properties, J. Mar. Chim. Heterocycl. 16 (1) (2017) 1–47. https://revues.imist.ma/index.php?journal=JMCH&page=article&op=view&path%5B%5D=8199&path%5B%5D=4629.

[32] S. De Vaugelade, E. Nicol, S. Vujovic, S. Bourcier, S. Pirnay, S. Bouchonnet, Ultraviolet–visible phototransformation of dehydroacetic acid – dtructural characterization of photoproducts and global ecotoxicity, Rapid Commun. Mass Spectrom. 32 (11) (2018) 862–870.

[33] M.V. Cooke, M.B. Oviedo, W.J. Peláez, G.A. Argüello, UV characterization and photodegradation mechanism of the fungicide chlorothalonil in the presence and absence of oxygen, Chemosphere 187 (2017) 156–162.

[34] N. Poisson, M. Kanakidou, P.J. Crutzen, Impact of non-methane hydrocarbons on tropospheric chemistry and the oxidizing power of the global troposphere: 3-dimensional modelling results, J. Atmos. Chem. 36 (2) (2000) 157–230.

[35] A. Vasiliou, M.R. Nimlos, J.W. Daily, G.B. Ellison, Thermal decomposition of furan generates propargyl radicals, J. Phys. Chem. A 113 (30) (2009) 8540–8547.

[36] T.L. Nguyen, B.C. Xue, G.B. Ellison, J.F. Stanton, Theoretical study of reaction of ketene with water in the gas phase: formation of acetic acid? J. Phys. Chem. A 117 (43) (2013) 10997–11005.